Mott-Hubbard quantum criticality in paramagnetic CMR pyrochlores

L. Craco,[1] C. I. Ventura,[2] A. N. Yaresko,[3] and E. Müller-Hartmann[1]
[1]*Institut für Theoretische Physik, Universität zu Köln, Zülpicher Straße 77, 50937 Köln, Germany*
[2]*Centro Atómico Bariloche, 8400 - Bariloche, Argentina*
[3]*Max-Planck-Institut für Physik Komplexer Systeme, Nöthnitzer Straße 38, 01187 Dresden, Germany*
(Received 25 January 2006; published 23 March 2006)

We present a correlated *ab initio* description of the paramagnetic phase of $Tl_2Mn_2O_7$, employing a combined local density approximation with multiorbital dynamical mean-field theory treatment. We show that the insulating state observed in this colossal magnetoresistance pyrochlore is determined by strong Mn intra- and inter-orbital local electron-electron interactions. Hybridization effects are reinforced by the correlation-induced spectral weight transfer. Our result coincides with optical conductivity measurements, whose low-energy features are well accounted for by our theory. We also study the disorder-driven insulator-metal transition of doped compounds, showing the proximity of $Tl_2Mn_2O_7$ to quantum phase transitions, in agreement with recent measurements.

DOI: 10.1103/PhysRevB.73.094432 PACS number(s): 75.47.Lx, 71.15.−m, 71.27.+a, 71.30.+h

I. INTRODUCTION

Among the manganese oxides exhibiting colossal magnetoresistance (CMR),[1] the family of pyrochlores represented by $Tl_2Mn_2O_7$,[2–4] and the related compounds prepared by substitution of its different components[3,5,6] stands out. Though presenting coupling between magnetic and transport properties similar to those of the CMR perovskite manganites such as $La_{1-x}A_xMnO_3$ ($A=$ Ca,Sr,Ba), in the last nine years, experiments have established many differences of their electronic properties,[2] lattice behavior,[2–4,7,8] spin dynamics,[9] etc. In particular, transport and magnetism in CMR pyrochlores seem to be related primarily to different electronic orbitals[4,5] coupled by hybridization. Mechanisms like double exchange, involving the transfer of electrons between neighbor Mn^{3+}-Mn^{4+} ions, which favors ferromagnetic alignment of the Mn core spins,[10] and effects like Jahn-Teller distortions,[11] were early discarded for pyrochlore compounds. A series of alternative theoretical proposals were put forward and explored in connection with the experimental results.[12–16]

The first microscopic model studied for $Tl_2Mn_2O_7$ was the intermediate valence model (IVM),[12] proposed to explore the suggestion[4] of the presence of a small effective internal doping of the type $Tl^{3+}_{2-x}Tl^{2+}_xMn^{4+}_{2-x}Mn^{5+}_xO_7$ ($x\sim 0.005$). The presence of spin-dependent hybridization gaps (or pseudogaps), and the predicted temperature and magnetic field dependent changes of the electronic structure allowed description of the observed magnetotransport.[12] In particular, the predicted evolution from a half-metallic ferromagnetic phase towards a gapped paramagnetic state above T_c explained the drastic reduction of the number of carriers at T_c in Hall data.[2,4] Majumdar and Littlewood[13] have explored the scenario of spin fluctuations around T_c in the presence of very low carrier densities, first suggested in Refs. 4 and 5. Considering Hund and superexchange couplings,[13] they explained CMR in terms of spin polarons. A ferromagnetic double-exchange Hamiltonian for $Tl_2Mn_2O_7$ with a small number of Zener carriers, which align antiparallel to the localized Mn t_{2g} spins, including a weak antiferromagnetic superexchange coupling between localized spins, has also been proposed.[14] An explanation for the origin and pressure dependence of ferromagnetism has been proposed using a ferromagnetic superexchange model,[15] provided strong intra-atomic Hund interactions in oxygen, and hybridization of the empty Mn e_g orbitals with O and Tl levels were considered. Later, a generic effective model for $Tl_2Mn_2O_7$ (see Ref. 16) was introduced to explore and compare various proposals.[2,4,13–15] Interestingly, its electronic structure was shown[16] to exhibit similar features to the IVM model,[12] for appropriate parameters, while the experimental spin dynamics[9] could be described[17] if ferromagnetic superexchange was assumed.[15] Recently, thermopower and optical conductivity were qualitatively described using the IVM.[18]

$Tl_2Mn_2O_7$ is cubic at room temperature, with an fcc ($Fd\bar{3}m$) arrangement (see Fig. 1) of corner-sharing Mn-O6

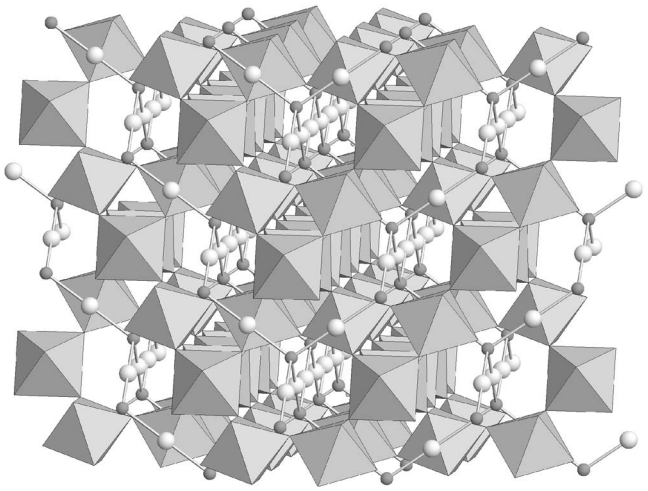

FIG. 1. Pyrochlore crystal structure: Tl and O are, respectively, represented by larger and small spheres (see Ref. 23). The Mn atoms are placed at the centers of the depicted Mn-O6 corner-sharing octahedra.

octahedra.[2,4] Its large magnetoresistance accompanies a ferromagnetic metal to paramagnetic insulator transition, with T_c around 130 K.[2–4] The magnetization below T_c is believed to be determined by ferromagnetic superexchange coupling in the Mn^{4+} sublattice.[4,15] Hall data indicate a very small electron-like carrier density[2] ($\sim 0.001-0.005\ e/\mathrm{f.u.}$), connected with the presence of extended Tl 6*s* orbitals hybridizing with O 2*p* and Mn t_{2g} states near the Fermi level.[14,19,20] Upon Bi substitution on the Tl site, magnetoresistance increases drastically and transport above T_c is strongly modified.[6] Notably, CMR is achieved at room temperatures, indicating the possibility of technological applications of $Tl_{2-x}Bi_xMn_2O_7$ and related compounds.

The electronic band structure of $Tl_2Mn_2O_7$ has been calculated in local density approximation (LDA) by various groups.[14,19,20] They obtained similar results for the ferromagnetic metallic ground state, characterizing it as a half-metal with minority-spin free-electron-like carriers. However, no attention has been paid to the paramagnetic (PM) phase. In this work, we are presenting the first *ab initio* study of the paramagnetic phase of $Tl_2Mn_2O_7$. We found that LDA calculations predict a metallic paramagnetic state, in contrast to recent optical conductivity[21] and photoemission[22] experiments clarifying its insulating nature. By including multiorbital correlations through a combination of LDA with dynamical mean-field theory (DMFT), we characterize the paramagnetic phase as a Mott-Hubbard insulator, with a correlation-induced gap. We calculated optical conductivity contributions, and discuss our results in the context of recent experiments[21,22] and effective model calculations.[12] Finally, we focus on the insulator-metal transition induced by chemical substitution.[6]

II. MODEL AND LDA+DMFT APPROACH

Let us briefly outline the scheme of electronic structure calculation used. LDA band structure calculations were performed for the experimental crystal structure of $Tl_2Mn_2O_7$ (see Ref. 20) using the LMTO method[24] in the atomic sphere approximation. The overlap of atomic spheres was decreased by adding two sets of empty spheres in 8*a* and 32*e* Wyckoff positions of the $Fd\bar{3}m$ space group. Our ferromagnetic phase results (not shown) agree with previous ones,[14,19,20] while the electronic structure obtained for the paramagnetic phase is shown in Fig. 2. The differentiated hybridization between Tl and Mn with the two kinds of O atoms present is evident. Clearly, a metallic paramagnetic state is predicted by LDA, in contradiction with the insulating behavior recently established experimentally.[21,22]

To include the real band structure and reliably treat the effect of correlations in the PM phase, as well as study metal-insulator transitions, we adopted the combined LDA+DMFT approach, which is becoming widely recognized as suitable for the realistic description of transition metal oxides.[25,26] Previous similar applications of the technique include, e.g., the study of the insulator-metal transition in V_2O_3 and the ferromagnetic metallic state of CrO_2.[27] The multiorbital many-body Hamiltonian considered for the LDA+DMFT study of $Tl_2Mn_2O_7$ is

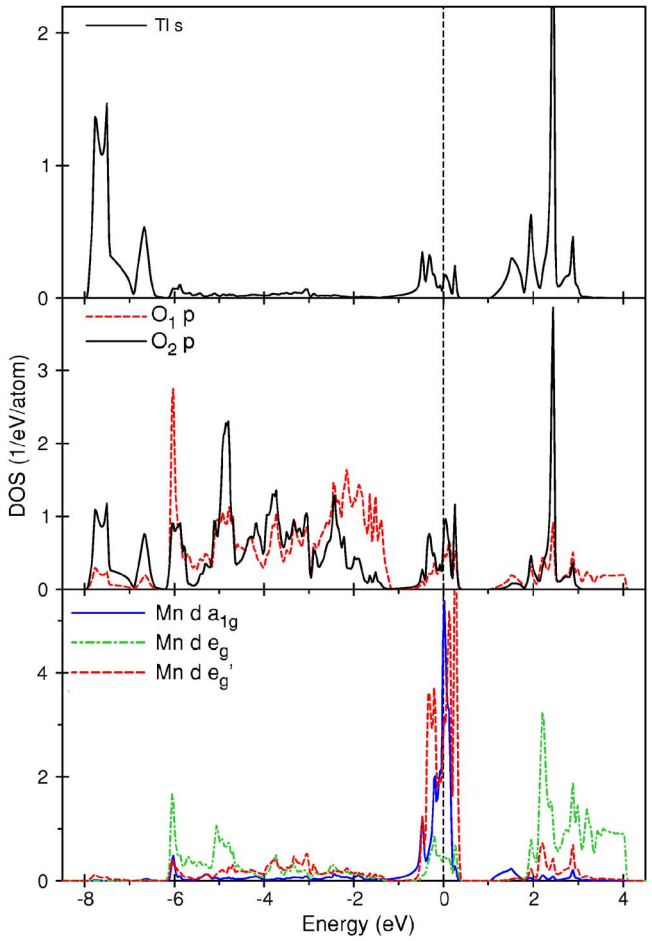

FIG. 2. (Color online) LDA band structure for paramagnetic $Tl_2Mn_2O_7$. $O_1(O_2)$ denotes oxygen ions nearest to Mn (Tl).

$$H = \sum_{\mathbf{k}\alpha\beta\sigma} (\epsilon_{\mathbf{k}\alpha} + \epsilon^0_\alpha \delta_{\alpha\beta}) c^\dagger_{\mathbf{k}\alpha\sigma} c_{\mathbf{k}\beta\sigma} + U \sum_{ia} n_{ia\uparrow} n_{ia\downarrow} + U' \sum_{i\alpha\neq\beta} n_{i\alpha} n_{i\beta} - J_H \sum_{i\alpha\neq\beta} \mathbf{S}_{i\alpha} \cdot \mathbf{S}_{i\beta}, \quad (1)$$

where α, β denote the three t_{2g} orbitals. Due to the pyrochlore crystal field, the t_{2g} subshell is split into an a_{1g} singlet and an e'_g doublet. The size of the splitting $\Delta = \delta_{e'_g} - \delta_{a_{1g}}$ (δ_α being the center of gravity of the α band) within LDA is: $\Delta_{\mathrm{LDA}} = 0.037$ eV. To avoid double counting of interactions included already in the LDA in average, ϵ^0_α reads; $\epsilon^0_\alpha = \epsilon_\alpha - U\left(n_{\alpha\bar{\sigma}} - \frac{1}{2} + \frac{J_H}{2}\sigma(n_{\alpha\sigma} - 1)\right)$, with ϵ_α being the on-site energies of the t_{2g} orbitals. The first term in Eq. (1) describes the one-electron part of the Hamiltonian, including details of the pyrochlore crystal structure of $Tl_2Mn_2O_7$ through the LDA band structure: $\epsilon_{\mathbf{k}\alpha}$. The next three terms account for local correlation effects in the t_{2g} orbitals. Notice that we are keeping only the t_{2g} orbitals since, from LDA, the density of states (DOS) for the e_g bands is small near the Fermi level $E_F(\equiv 0)$, the *O* 2*p* bands lie approximately 1.5 eV below E_F and the Tl 6*s* band about 2.5 eV above E_F. $U(U')$ denotes the t_{2g} intra- (inter-) orbital local Coulomb interaction. The last term in Eq. (1) describes the Hund's rule coupling: being

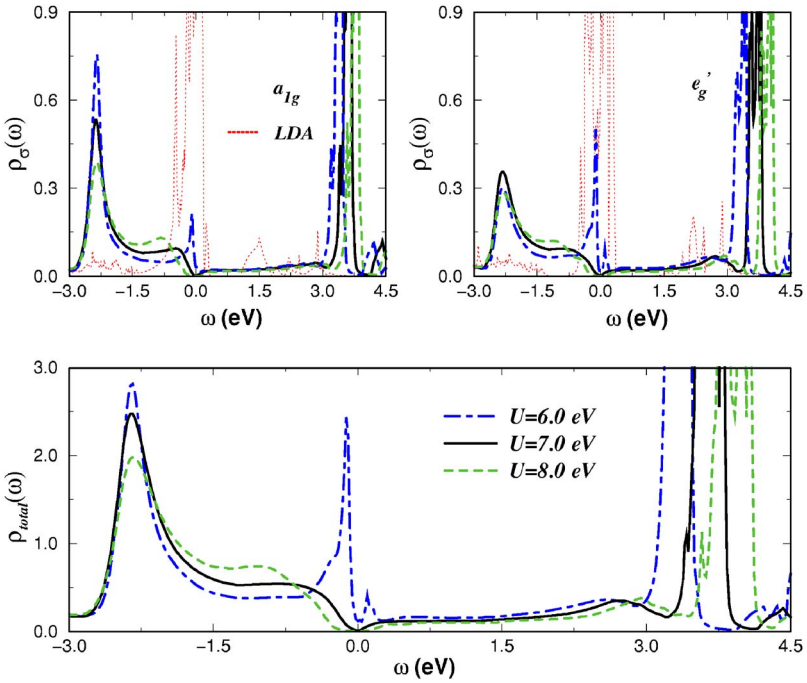

FIG. 3. (Color online) LDA+DMFT (paramagnetic $Tl_2Mn_2O_7$): orbital-resolved (upper panels) and total (lower panel) Mn densities of states, for $U=6.0$, 7.0, 8.0 eV, $J_H=1$ eV.

J_H poorly screened, we take it of the order of its atomic value in Mn^{4+}, $J_H=1$ eV. Rotational invariance fixes: $U'=U-2J_H$.[28]

We calculate the Green's functions of the Hamiltonian of Eq. (1) in $d=\infty$ using multiorbital iterated perturbation theory (MO-IPT).[27] Assuming no symmetry breaking in the spin/orbital sector, we have $G_{\alpha\beta\sigma\sigma'}(\omega)=\delta_{\alpha\beta}\delta_{\sigma\sigma'}G_{\alpha\sigma}(\omega)$ and $\Sigma_{\alpha\beta\sigma\sigma'}(\omega)=\delta_{\alpha\beta}\delta_{\sigma\sigma'}\Sigma_{\alpha\sigma}(\omega)$. The DMFT solution involves (i) replacing the lattice model by a self-consistently embedded multiorbital, asymmetric Anderson impurity model, and, (ii) a self-consistency condition requiring the local impurity Green's function to be equal to the local Green function for the lattice, i.e.,

$$G_\alpha(\omega)=\frac{1}{N}\sum_{\mathbf{k}}\frac{1}{\omega+\mu-\Sigma_\alpha^{int}[\omega,\mathcal{A}_\alpha(\omega)]-\epsilon_{\mathbf{k}\alpha}}$$
$$=\frac{1}{\omega+\mu-\Sigma_\alpha^{int}[\omega,\mathcal{A}_\alpha(\omega)]-\mathcal{A}_\alpha(\omega)}. \quad (2)$$

with $\mathcal{A}_\alpha(\omega)$ being the dynamical Weiss field for orbital α. The calculation for $\Sigma_\alpha^{int}(\omega)$ follows the philosophy of the one-orbital IPT, with the Green functions and self-energies being matrices in the orbital indices. The equations for the MO-IPT ($\Sigma_\alpha^{int}\equiv\Sigma_\alpha^{\text{MO-IPT}}$) are the same as used before.[27,29] They are solved self-consistently with the LDA density of states as input, until convergence is achieved. Local self-energies computed from the MO-IPT do exactly satisfy the Friedel-Luttinger sum rule, guaranteeing the correct low-energy form of the spectral function. The correct high-energy behavior is ensured by the self-consistent determination of the first few moments of the spectral function.

III. RESULTS AND DISCUSSION

A. Correlation effects

We now present our LDA+DMFT results. In Fig. 3 we plot the t_{2g} density of states of the Mn ions. We show results for different values of the Coulomb interactions corresponding to two distinct correlated phases; i.e., below and above the metal-insulator transition point. For $U=6.0$ eV and $U'=U-2J_H=4.0$ eV as intra- and interorbital correlation values, we obtain finite density of states at the Fermi level. On the other hand, for both $U=7.0$ eV and $U=8.0$ eV, we see a clear Mott-Hubbard insulating state with an energy gap at the Fermi level. As expected the Mott-Hubbard gap increases with U. Compared to the LDA results of Fig. 2 the correlated DOS shows that spectral weight has been transferred to energies close to maxima of the Tl and O bands, therefore reinforcing hybridization effects. In view of this, one may envisage an overall gapped (insulating) state resulting from rehybridization, in a scenario with common features to those predicted by the effective IVM for paramagnetic $Tl_2Mn_2O_7$.[12] The occupations of the respective t_{2g} orbitals obtained from the converged solution of the dynamical mean-field equations for $U=7.0$ eV are $[(n_{a_{1g}},n_{e_g'},n_{e_g'})=(1.06,1.04,1.04)]$, consistent with having a $S=3/2$ spin state (corresponding to Mn^{4+}).

As seen in Fig. 3, a large amount of spectral weight is transferred to the Hubbard satellites located at energies of about 3.0 eV. Here, due to strong multiorbital electron interactions it is possible to resolve both U and U' Hubbard satellites. For $U=7$ eV the former are located at about -2.42 and 3.58 eV. The interorbital Hubbard satellites are distinguishable only in the upper part of the spectra, as the lower ones overlap with the incoherent part originated from U; e.g., within the e_g' sector the U'-satellites are visible at energies of about 2.65 eV. Recent photoemission experiments at room

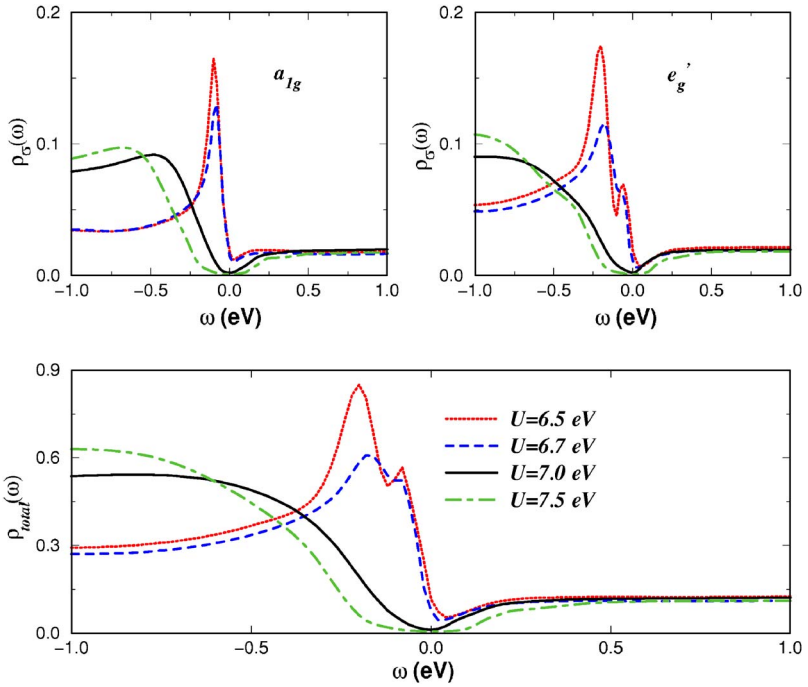

FIG. 4. (Color online) Low-energy view of LDA+DMFT orbital-resolved (upper panels) and total (lower panel) DOS, for $J_H=1.0$ eV and values of U below and above the metal-insulator transition point.

temperature[22] have confirmed the insulating nature of the paramagnetic phase. Finding a higher weight for O $2p$ at the upper edge of the valence band, in Ref. 22, $Tl_2Mn_2O_7$ is characterized as a charge-transfer insulator. Strong hybridization of O $2p$ and Mn t_{2g} in the valence band is reported, and a 2–3 eV difference between the centers of gravity of the respective bands is estimated: the Mn one lying mainly at binding energies above 3 eV.[22] Interestingly, the correlation-induced shift of Mn spectral weight we find with respect to the LDA, goes in the same direction: shifting the center of gravity of the Mn valence band towards higher binding energies.

Additionally, Ref. 22 characterizes $Tl_2Mn_2O_7$ as close to a metal-insulator transition. With this in mind, we show in Fig. 4 the effect of $U(U')$ near the metal-insulator transition point. Below $U=6.7$ eV the hypothetical paramagnetic metallic phase (which is never observed in reality for the stoichiometric compound) shows an asymmetric but sharp, quasicoherent Fermi liquid-like resonance below 0.05 eV binding energy. Such an asymmetric profile is known to occur and has been obtained for a host of correlated electronic systems within the LDA+DMFT scheme.[26,30] The first order metal-insulator transition is found to take place between $6.7<U<7.0$ eV, i.e., inside the expected range: since for all $3d$ metals the value of U has been predicted to vary between 2 and 6–7 eV.[25,26,30] For U of about 7.0 eV, a clear Mott-Hubbard insulating state is obtained and the charge gap increases with U. At this point it is convenient to mention that to obtain a correlated Mott insulator in multiorbital systems, we need both U and $U' \simeq (U-2J_H)$. In a situation where U' is absent, a t_{2g} electron hopping from one Mn site to its neighbor could hop off like a band electron just by going into a virtually unoccupied t_{2g} orbital at that site, making a paramagnetic insulating state almost impossible.[31] Taken together, our results shown in Figs. 3 and 4 account for a systematic evolution of the one-particle spectra for $3d^3$ pyrochlore oxides.

To compare our theoretical findings with experimental data, we evaluate the t_{2g} contribution to the optical conductivity in the paramagnetic insulating phase. In what follows, we consider only the t_{2g} intraband optical transitions: due to orthogonality of these orbitals, one would expect negligible contributions from interband transitions.[32] Within the t_{2g} subshell, the contributions to optical conductivity are calculated from

$$\sigma(\omega) \propto \sum_{\alpha \mathbf{k}} \int d\omega' A_{\alpha\mathbf{k}}(\omega') A_{\alpha\mathbf{k}}(\omega'+\omega) \frac{(f(\omega')-f(\omega+\omega'))}{\omega} \tag{3}$$

where $f(\omega)$ is the Fermi function and $A_\alpha(\mathbf{k},\omega)=\frac{1}{\pi}\,\mathrm{Im}[\omega - \Sigma_\alpha(\omega)-\epsilon_{\alpha\mathbf{k}}]^{-1}$ is the spectral density.

In Fig. 5 we show the calculated optical conductivity together with the experimental data at room temperature.[21] Apart from the visible small peaks related to phonons (not included in our treatment), good quantitative agreement is found at low energies (below 0.8 eV). We are not including phonons for our study of electronic properties based on the experimental evidence: recent detailed lattice dynamical studies with Raman and IR spectroscopy for $Tl_2Mn_2O_7$ (see Ref. 8) have confirmed the lack of any important electron-phonon coupling, in agreement with early reports.[2–4,7] The absence of optical response observed at very low energies in $Tl_2Mn_2O_7$ evidences the insulating nature of the paramagnetic phase. As one can see in Fig. 5, much better agreement is obtained for $U=7.0$ eV than for $U=7.5$ eV, indicating that the Mott-Hubbard gap is really very small in $Tl_2Mn_2O_7$. For higher energies, a quantitative description of experiments would require to include the effect of interband charge-transfer excitations, from O $2p$ and Tl s to Mn $3d$ bands, out of the scope of the present work.

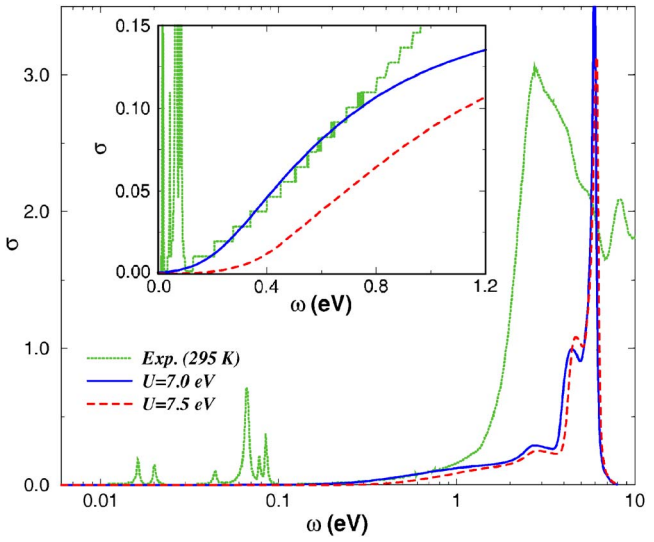

FIG. 5. (Color online) Paramagnetic $Tl_2Mn_2O_7$: t_{2g} optical conductivity calculated with LDA+DMFT for $U=7.0$ eV and $U=7.5$ eV, compared with experiment at $T=295$ K (see Ref. 21). Inset: Low-energy conductivity: LDA+DMFT vs experiment at $T=295$ K.

B. Disorder effects

In this section we address the effect of disorder induced by chemical substitution.[6] The problem is treated within the LDA+DMFT(IPT+CPA) approach, which treats disorder exactly in high dimensions and has been used, for example, to describe the doping-driven insulator-metal transition in $LaTiO_3$ (see Ref. 33) and the effect of disordered Jahn-Teller distortions in half-metallic ferromagnetic three-dimensional manganites.[29] This scheme is an extension of that applied to the one-band disordered Hubbard model,[34] where the effect of site-diagonal disorder is accounted for by adding $H_d = \Sigma_{i\alpha\sigma} v_i n_{i\alpha\sigma}$ to Eq. (1). In the spirit of Refs. 34 and 35, we restrict ourselves to a binary-alloy distribution for disorder, therefore the disorder potentials v_i are specified by the probability distribution

$$P(v_i) = (1-x)\,\delta(v_i) + x\,\delta(v_i - v), \tag{4}$$

meaning that upon doping or chemical substitution a fraction x of sites have an additional local potential v for an electron (or hole) hopping onto that site. In other words, the carriers experience different local environments in the course of their hopping, and the physical object which accounts for this effect is the disorder-averaged local Green's function, $\langle G(\omega)\rangle_{ii}$, $\langle..\rangle_{ii}$ denoting the disorder average. After configurational averaging using T-matrix approximation, all interesting dynamical effects are contained in the coherent potential approximation (CPA) self-energy

$$\Sigma_\alpha^{\mathrm{CPA}}(\omega) = xv + \frac{v^2 x(1-x)}{\omega - v(1-x) - \mathcal{A}_\alpha(\omega)} \tag{5}$$

related to the single-site (CPA) propagator

$$\langle G_\alpha(\omega)\rangle_{ii} = \frac{1-x}{\omega - \mathcal{A}_\alpha(\omega)} + \frac{x}{\omega - v - \mathcal{A}_\alpha(\omega)}. \tag{6}$$

Here, the dynamical Weiss function $\mathcal{A}_\alpha(\omega)$ describes the motion of α-band electrons in the effective medium related to disorder.

The combined $U+v$ (Mott-Anderson) problem, i.e., the situation where strong electronic correlations and disorder-induced scattering processes simultaneously affect the one-particle response, is treated in $d=\infty$ by a proper combination of the interaction self-energy with the CPA one[29,34]

$$G_\alpha(\omega) = \frac{1}{N}\sum_{\mathbf{k}} \frac{1}{\omega - \Sigma_\alpha^{int}(\omega) - \Sigma_\alpha^{\mathrm{CPA}}(\omega) - \epsilon_{\mathbf{k}\alpha}}. \tag{7}$$

Solution of Eq. (7) gives the total self-energy $\Sigma_\alpha = \Sigma_\alpha^{int} + \Sigma_\alpha^{\mathrm{CPA}}$ corrected simultaneously for scattering caused by electron correlations (MO-IPT) and disorder (CPA). Here, disorder and Coulomb interactions are represented by different self-energies that result in new local and lattice Green's functions $[G_\alpha(\omega)]$, as well as the new dynamical Weiss functions. The latter are fed back into both modified CPA and MO-IPT self-energies, and the procedure is iterated until self-consistency is reached.

To proceed with the $U+v$ problem, we would like to notice that differently from Ref. 33, we will consider here only the effect of substitutional disorder: without the introduction of extra holes or electrons in the system. By this, we aim to account for a host of experimental realizations in the limit of small impurity concentrations.[36] Having in mind the possibility of technological applications upon Bi substitution,[6] in our calculation we use a disorder potential $v=2.5$ eV, corresponding to the energy difference between the Tl $6s$ band and the Bi $6p$ band.[37]

In Figs. 6 and 7 we illustrate the effect of disorder on our results for $U=7.0$ eV. Figure 6 shows that introduction of a small amount of impurities metallizes the system, in agreement with Refs. 6 and 36. Due to the pyrochlore structure, the Mott-Hubbard insulating state seems to be very unstable, allowing for first-order insulator-metal transitions upon small perturbations. According to our results, disorder or chemical pressure may drive $Tl_2Mn_2O_7$ into a bad metal fixed point, similar to that obtained for values of U corresponding to the metallic phase discussed before. As expected from general grounds within the DMFT framework,[31,33] we observe a closing of the Mott-Hubbard gap by incoherent spectral weight transferred across large energy scales. However, differently from previous calculations using the same approach,[31] the multiorbital Kondo-like resonance appearing just below the Fermi level increases with x. This type of evolution of the Kondo-screening cloud indicates that there might be a fundamental difference of the effect of disorder in $3d^3$ pyrochlore structures compared to other types of t_{2g} systems. It seems that the interplay between disorder and Coulomb interactions can be very subtle in this class of electronic systems. Here, the character of the metallic state itself, as well as details of the actual one-particle spectrum depend sensitively on how the Mott-Hubbard localization is affected by disorder. In our view the disordered metallic state derived

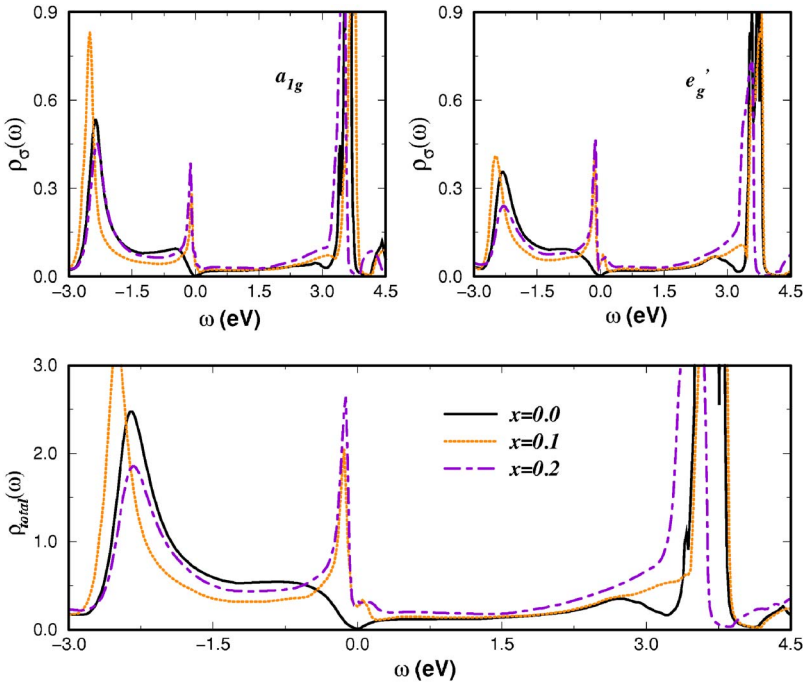

FIG. 6. (Color online) Effect of disorder: orbital-resolved (upper panels) and total (lower panel) DOS for $Tl_{2-x}Bi_xMn_2O_7$. $U=7.0$ eV and $v=2.5$ eV.

above results from an instability of the correlated Mott insulating state. Contrary to naive expectation, Fig. 6 demonstrates that the disorder-driven insulator-to-metal transition in $Tl_{2-x}Bi_xMn_2O_7$ is of the first order type and it is not simply accompanied by a smooth crossover as it is known to occur, for example, in Sr-doped $LaTiO_3$.[33]

To demonstrate that our approach correctly accounts for the effect of Coulomb interactions in the disorder-driven metallic phase of Bi-doped $Tl_2Mn_2O_7$, we analyze in Fig. 7 the evolution of this metallic state for two values of U. Clearly, our result follows the trend of correlated multiorbital systems treated within DMFT. As expected, the resonance below the Fermi level is lowered in height and its spectral weight is reduced by U. In addition, the Hubbard satellites are transferred to higher energies. It follows from this result that disorder or chemical pressure may induce electron screening. Therefore, the $U+v$ metallic phase obtained here points towards a different class of Mott-Anderson systems,[38] where disorder may not induce Anderson localization.

The above results highlight the basic feature that may aid the design of new materials close to magnetic or charge/orbital instabilities. What is of great importance in our theory of disorder-driven quantum critical instabilities is that we identify the regime of (material specific) parameters in which (controlled) calculations based on LDA+DMFT (IPT+CPA)[31,33] are possible. We found a totally different re-

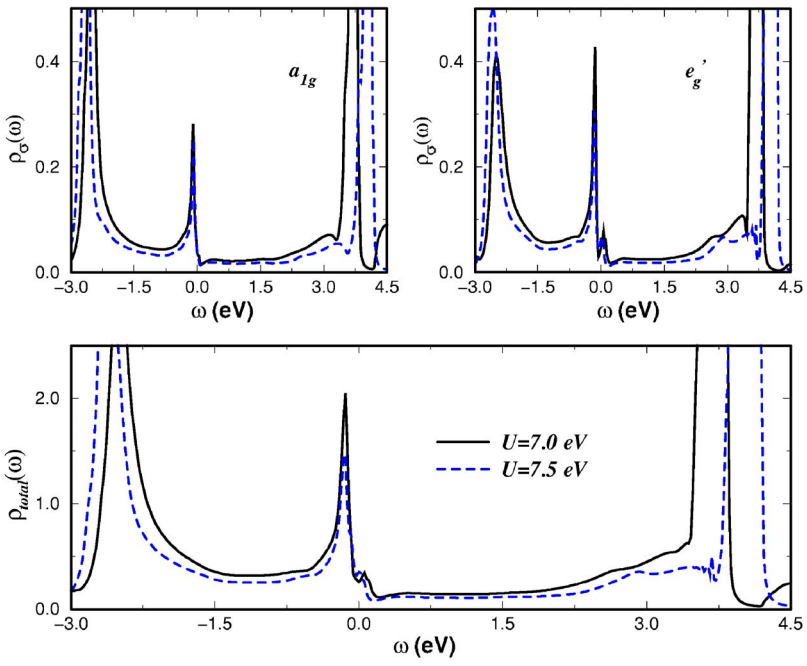

FIG. 7. (Color online) Effect of U in the disordered system: orbital-resolved (upper panels) and total (lower panel) DOS for $x=0.1$, $v=2.5$ eV, and two values of U.

sponse for the one-particle spectra due to non trivial interplay between disorder and electron correlations in geometrically frustrated pyrochlores. The tiny charge gap induced by strong dynamical electron interactions in the vicinity of half-filling is a crucial attribute for $Tl_2Mn_2O_7$ to be close to a quantum critical regime. Here, we would like to add that, it is a real theoretical challenge to understand the effect of disorder on the Mott-Hubbard insulating state of multiorbital systems. Therefore, the critical character of the Mott transition illustrated in Fig. 6 may open a novel scenario in frustrated lattices and future investigations should focus on distinct responses in the full v, x, and electron-filling phase diagram, where different phases (spin-glass freezing, phase separation,[39] etc.) are expected. The endeavor to explain $Tl_2Mn_2O_7$ is in progress.

IV. CONCLUSIONS

To conclude, we have presented an *ab initio* study of the paramagnetic phase of $Tl_2Mn_2O_7$. Through the inclusion of local multiorbital Coulomb interactions and using a combined LDA+DMFT approach, we describe the insulating nature of this phase. Hybridization effects are reinforced by the spectral weight transfer due to strong correlations. The electronic structure obtained with $U=7$ eV allows us to provide not only a consistent description of the low-energy optical conductivity data, but also a support for our picture of disorder effects induced by chemical substitution. In agreement with chemical doping studies and recent photoemission findings, our results indicate that $Tl_2Mn_2O_7$ is very near to quantum phase instabilities, and illustrate the interplay of strong multiorbital correlations with disorder and pyrochlore structure effects, thus calling for investigation with higher resolution spectroscopies, including inverse photoemission.

ACKNOWLEDGMENTS

We benefited from discussions with D.I. Khomskii and M.S. Laad. C. I. V. also thanks B. Alascio, J.A. Alonso, M. Foglio, M.N. Regueiro and G. Zampieri for comments and references. L. C. was supported by the SFB 608 of the Deutsche Forschungsgemeinschaft. C. I. V. is Investigador Científico of CONICET (Argentina), and thanks CONICET/DAAD (Deutscher Akademischer Austauschdienst) for financial support and the Institut für Theoretische Physik, Universität zu Köln, for the hospitality.

[1] H. Kuwahara and Y. Tokura, in *Colossal Magnetoresistance, Charge Ordering and Related Properties of Manganese Oxides*, edited by C. N. R. Rao and B. Raveau (World Scientific, Singapore, 1998).
[2] Y. Shimakawa, Y. Kubo, and T. Manako, Nature (London) **379**, 55 (1996).
[3] S. W. Cheong, H. Y. Hwang, B. Batlogg, and L. W. Rupp, Jr., Solid State Commun. **98**, 163 (1996).
[4] M. A. Subramanian, B. H. Toby, A. P. Ramirez, W. J. Marshall, A. W. Sleight, and G. H. Kwei, Science **273**, 81 (1996).
[5] A. P. Ramirez and M. A. Subramanian, Science **277**, 546 (1997).
[6] J. A. Alonso, J. L. Martínez, M. J. Martínez-Lope, M. T. Casais, and M. T. Fernández-Díaz, Phys. Rev. Lett. **82**, 189 (1999).
[7] Y. Shimakawa, Y. Kubo, T. Manako, Y. V. Sushko, D. N. Argyriou, and J. D. Jorgensen, Phys. Rev. B **55**, 6399 (1997); see also G. H. Kwei, C. H. Booth, F. Bridges, and M. A. Subramanian, *ibid.* **55**, R688 (1997).
[8] S. Brown, H. C. Gupta, J. A. Alonso, and M. J. Martínez-Lope, Phys. Rev. B **69**, 054434 (2004).
[9] J. W. Lynn, L. Vasiliu-Doloc, and M. A. Subramanian, Phys. Rev. Lett. **80**, 4582 (1998).
[10] C. Zener, Phys. Rev. **82**, 403 (1951); P. W. Anderson and H. Hasegawa, *ibid.* **100**, 675 (1955); P. G. de Gennes, *ibid.* **118**, 141 (1960).
[11] A. J. Millis, P. B. Littlewood, and B. I. Shraiman, Phys. Rev. Lett. **74**, 5144 (1995); A. J. Millis, B. I. Shraiman, and R. Mueller, *ibid.* **77**, 175 (1996).
[12] C. I. Ventura and B. Alascio, Phys. Rev. B **56**, 14533 (1997).
[13] P. Majumdar and P. Littlewood, Phys. Rev. Lett. **81**, 1314 (1998).
[14] S. K. Mishra and S. Satpathy, Phys. Rev. B **58**, 7585 (1998).
[15] M. D. Núñez-Regueiro and C. Lacroix, Phys. Rev. B **63**, 014417 (2001).
[16] C. I. Ventura and M. A. Gusmão, Phys. Rev. B **65**, 014422 (2002).
[17] C. I. Ventura and M. Acquarone, Phys. Rev. B **70**, 184409 (2004).
[18] M. E. Foglio and G. E. Barberis, Phys. Rev. B **72**, 125129 (2005).
[19] D. J. Singh, Phys. Rev. B **55**, 313 (1997).
[20] Y. Shimakawa, Y. Kubo, N. Hamada, J. D. Jorgensen, Z. Hu, S. Short, M. Nohara, and H. Takagi, Phys. Rev. B **59**, 1249 (1999).
[21] H. Okamura, T. Koretsune, M. Matsunami, S. Kimura, T. Nanba, H. Imai, Y. Shimakawa, and Y. Kubo, Phys. Rev. B **64**, 180409(R) (2001).
[22] J. Sánchez-Benítez, A. de Andrés, C. Prieto, J. Ávila, L. Martín-Carrón, J. L. Martínez, J. A. Alonso, M. J. Martínez-Lope, and M. T. Casais, Appl. Phys. Lett. **84**, 4209 (2004).
[23] V. V. Nemoshkalenko, S. V. Borisenko, V. N. Uvarov, A. N. Yaresko, A. G. Vakhney, A. I. Senkevich, T. N. Bondarenko, and V. D. Borisenko, Phys. Rev. B **63**, 075106 (2001).
[24] O. K. Andersen, Phys. Rev. B **12**, 3060 (1975).
[25] G. Kotliar and D. Vollhardt, Phys. Today **57**(3), 53 (2004).
[26] See G. Kotliar, S. Y. Savrasov, K. Haule, V. S. Oudovenko, O. Parcollet, and C. A. Marianetti, cond-mat/0511085 (unpublished), and references therein.
[27] L. Craco, M. S. Laad, and E. Müller-Hartmann, Phys. Rev. Lett. **90**, 237203 (2003); M. S. Laad, L. Craco, and E. Müller-Hartmann, *ibid.* **91**, 156402 (2003).
[28] K. Held and D. Vollhardt, Eur. Phys. J. B **5**, 473 (1998).
[29] M. S. Laad, L. Craco, and E. Müller Hartmann, New J. Phys. **6**, 157 (2004).
[30] L. Chioncel, E. Arrigoni, M. I. Kastneltson, and A. I. Lichtenstein, cond-mat/0601376 (unpublished).
[31] M. S. Laad, L. Craco, and E. Müller-Hartmann, Phys. Rev. B **73**,

045109 (2006).
[32] E. Pavarini, A. Yamasaki, J. Nuss, and O. K. Andersen, New J. Phys. **7**, 188 (2005); http://stacks.iop.org/1367-2630/7/188
[33] L. Craco, M. S. Laad, S. Leoni, and E. Müller-Hartmann, Phys. Rev. B **70**, 195116 (2004).
[34] M. S. Laad, L. Craco, and E. Müller-Hartmann, Phys. Rev. B **64**, 195114 (2001).
[35] K. Byczuk, W. Hofstetter, and D. Vollhardt, Phys. Rev. B **69**, 045112 (2004); see also, P. Lombardo, R. Hayn, and G. I. Japaridze, cond-mat/0512702 (unpublished).
[36] P. Velasco, J. A. Alonso, M. J. Martínez-Lope, M. T. Casais, and J. L. Martínez, J. Magn. Magn. Mater. **242**, 725 (2002); P. Velasco, J. A. Alonso, V. G. Tissen, W. G. Marshall, M. T. Casais, M. J. Martínez-Lope, A. de Andrés, C. Prieto, and J. L. Martínez, Phys. Rev. B **67**, 104403 (2003).
[37] J. Park, K. H. Kim, Han-Jin Noh, S.-J. Oh, J.-H. Park, Hong-Ji Lin, and C.-T. Chen, Phys. Rev. B **69**, 165120 (2004).
[38] D. Belitz and T. R. Kirkpatrick, Rev. Mod. Phys. **66**, 261 (1994); P. A. Lee and T. V. Ramakrishnan, *ibid.* **57**, 287 (1985); P. Majumdar and S. Kumar, Phys. Rev. Lett. **90**, 237202 (2003).
[39] P. Velasco, J. Mira, F. Guinea, J. Rivas, M. J. Martínez-Lope, J. A. Alonso, and J. L. Martínez, Phys. Rev. B **66**, 104412 (2002).